Low Temperature Physics/Fizika Nizkikh Temperatur, 2016, v. 42, No. 8, pp. 792–808

Physics of solid–liquid interfaces: from the Young equation to the superhydrophobicity

(Review Article)

Edward Bormashenko

Ariel University, Natural Science Faculty, Physics Department, P.O.B. 3, 407000, Ariel, Israel
E-mail: edward@ariel.ac.il

Received March 10, 2016, published online June 24, 2016

The state-of-art in the field of physics of phenomena occurring at solid/liquid interfaces is presented. The notions of modern physics of wetting are introduced and discussed including: the contact angle hysteresis, disjoining pressure and wetting transitions. The physics of low temperature wetting phenomena is treated. The general variational approach to interfacial problems, based on the application of the transversality conditions to variational problems with free endpoints is presented. It is demonstrated that main equations, predicting contact angles, namely the Young, Wenzel and Cassie–Baxter equations arise from imposing the transversality conditions on the appropriate variational problem of wetting. Recently discovered effects such as superhydrophobicity, the rose petal effect and the molecular dynamic of capillarity are reviewed.

PACS: 68.08.Bc Wetting;
68.08.–p Liquid–solid interfaces.

Keywords: capillarity, interface, superhydrophobicity, rose petal effect, Young equation, wetting.

Contents

1. Introduction

The center of mass of research activity of physicists, chemists and material scientists shifted markedly in the second half of the XX century from the study of bulk properties of materials to the processes occurring at interfaces. It turned out that interfacial processes govern to the much extent physical phenomena occurring not only in the nearest vicinity of a surface but also in the bulk of materials. It is noteworthy, that interfacial phenomena already attracted the attention of ancient natural philosophers. Plinius the elder, reported that vegetable oils poured on the surface of a rough sea have a calming effect on waves [1]. In the realm of classical physics such giants as B. Franklin, Lord Rayleigh and W. Thomson studied capillarity and wetting [2–4].

The situation changed, when ideas of modern physics formed the novel style of the scientific thinking. The field of wetting remained unattractive for young scientists for a long time, and this is in spite of the fact that Einstein, Shrödinger and Bohr devoted their research activity to this class of effects [5–8]. Einstein treated the origin of surface waves [6]. Shrödinger and Bohr suggested the witty methods of measurement of a surface tension of liquids [7,8]. It has been latently supposed that only physics of particles and phenomena occurring in a micro-world deserve the attention of inquisitive minds. Several factors have revived recently an interest in wetting and wettability. The first of these was the discovery of the "lotus" effect (or superhydrophobicity) by Barthlott and Neinhuis in 1997 [9]. The second factor was the rapid progress achieved in the field of wetting by the scientific school leaded by P.G. de Gennes [10]. It is noteworthy that the main notions of the modern theory of wetting (such as disjoining pressure, superhydrophobicity, contact angle hysteresis, wetting transitions) are younger than the basic ideas of relativity and quantum mechanics. Hence, the field of wetting phenomena is a rapidly developing field of modern physics, full of exciting physical insights.

The presented review is devoted to physics of solid-liquid interfaces, and more particularly to the applications of variational principles to wetting problems. Exploiting variational principles allows natural construction of a general umbrella enclosing a broad variety of wetting effects [11,12]. The review demonstrates that the well-known Young, Neumann–Boruvka, Cassie–Baxter and Wenzel equations actually represent the boundary transversality conditions for the appropriate problem of wetting [12].

2. Wetting of ideal surfaces

2.1 Wetting of flat ideal surfaces

Wetting is the ability of a liquid to maintain contact with a solid surface, resulting from intermolecular interactions when the two are brought together. The idea that wetting of solids depends on the interaction between particles

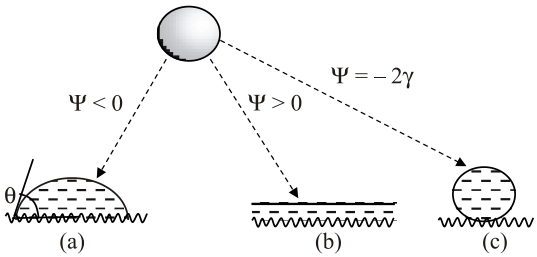

Fig. 1. The three wetting scenarios for sessile drops: partial wetting (the apparent contact angle θ is shown) (a); complete wetting (b); complete dewetting (also called superhydrophobicity) (c).

constituting a solid substrate and liquid has been expressed explicitly in the famous essay by Thomas Young [13]. When a liquid drop is placed on the solid substrate, two main static scenarios are possible: either liquid spreads completely, or it sticks to the surface and forms a cap as shown in Fig. 1(a) (a solid surface may be flat or rough, homogenous or heterogeneous). Fig. 1(a) also depicts the apparent contact angle θ, which serves as a natural macroscopic parameter of wetting. The precise definition of the apparent contact angle will be given in the Sec. 3.3; at this stage we only require that the radius of the droplet should be much larger than the characteristic scale of the surface roughness. The observed wetting scenario is dictated by a spreading parameter

$$\Psi = \hat{G}^*_{SA} - (\hat{G}^*_{SL} + \hat{G}_{LA}) , \qquad (1)$$

where $\hat{G}^*_{SA}$ and $\hat{G}^*_{SL}$ are the specific surface energies at the rough solid/air and solid/liquid interfaces (the asterisk reminds us that $\hat{G}^*_{SA}$ and $\hat{G}^*_{SL}$ do not coincide with the specific surface energies of smooth surfaces $\hat{G}_{SA}, \hat{G}_{SL}$), and $\hat{G}_{LA} = \gamma$ is the specific energy of the liquid/air interface. When $\Psi > 0$, total wetting is observed, depicted in Fig. 1(b). The liquid spreads completely in order to lower its surface energy (θ = 0). When $\Psi < 0$, the droplet does not spread but forms a cap resting on a substrate with a contact angle θ, as shown in Fig. 1(a). This case is called *partial wetting*. When the liquid is water, surfaces demonstrating $\theta < \pi/2$ are called *hydrophilic*, while surfaces characterized by $\theta > \pi/2$ are referred as *hydrophobic*. One more extreme, exotic situation is possible, when $\cos\theta = -1$, such as depicted in Fig. 1(c). This is the situation of complete dewetting or superhydrophobicity (reported first in Ref. 9) to be discussed in detail in the Sec. 4.1. When the solid surface is atomically flat, chemically homogeneous, isotropic, insoluble, non-reactive and non-stretched (thus, there is no difference between the specific surface energy and surface tension, the spreading parameter obtains its convenient form (see Ref. 10):

$$\Psi = \gamma_{SA} - (\gamma_{SL} + \gamma) , \qquad (2)$$

where $\gamma_{SA}, \gamma_{SL}, \gamma$ are the surface tensions at the solid/air (vapor), solid/liquid and liquid/air interfaces respectively [10]. When the droplet forms a cap, the line at which solid, liquid and gaseous phases meet is called *the triple* (or three phase) *line*.

Consider wetting of an ideal substrate in the situation of the partial wetting when $\Psi < 0$. When a droplet is deposited on such an ideal substrate as described in Fig. 2. its free energy G could be written as:

$$G[h(x,y)] = \iint_S \left[\gamma\sqrt{(1+(\nabla h)^2} + (\gamma_{SL} - \gamma_{SA})\right] dxdy \,, \quad (3)$$

where $h(x,y)$ is the local height of the liquid surface above the point (x,y) of the substrate (it is supposed latently that there is no difference between surface tensions and surface energies for γ_{SL}, γ_{SA}), and the integral is extended over the substrate area. The first term of the integrand presents the capillary energy of the liquid cap and the second term describes the change in the energy of the solid substrate covered by liquid.

Now we want to complicate the situation and expose our droplet to an external field. We restrict ourselves with an axially symmetrical situation depicted in Fig. 2, thus the interaction of the droplet with the field is described by the linear density $U(x, h(x))$ of the additional energy with the dimension of (J/m) $U(x,h(x)) = \int_0^{h(x)} 2\pi x w(x,y)dy$, where $w(x,y)$ is the volume energy density of the droplet in the external field. The functions $w(x,y)$ and $U(h(x),x)$ are dictated by the external field and are supposed to be known (for example, for a uniform gravity field $w = \rho g y/2$, $U(x,h(x)) = (x/2)\pi\rho g h^2(x)$, where ρ is the density of the liquid). Finally, the free energy of the droplet will be given by:

$$G(h,h') = \int_o^a \left[2\pi\gamma x\sqrt{1+h'^2} + 2\pi x(\gamma_{SL} - \gamma_{SA}) + U(x,h)\right] dx \,, \quad (4)$$

where $h' = dh/dx$, and a is the contact radius, shown in Fig. 2. We also suppose that the droplet does not evaporate, thus the condition of the constant volume V should be considered as:

$$V = \int_o^a 2\pi x h(x)dx = \text{const} \,. \quad (5)$$

If we want to calculate the shape of the droplet, Eqs. (4),(5) will reduce the problem to minimization of the functional:

$$G(h,h') = \int_0^a \tilde{G}(h,h',x)dx \,, \quad (6)$$

$$\tilde{G}(h,h',x) = 2\pi\gamma x\sqrt{1+h'^2} + 2\pi x(\gamma_{SL} - \gamma_{SA}) + U(x,h) + 2\pi\lambda x h \,, \quad (7)$$

where λ is the Lagrange multiplier to be deduced from Eq. (5). For a calculation of the droplet's shape we would have to solve the appropriate Euler–Lagrange equations [11]. However, we will not focus on the calculation of the droplet's shape, since our interest is the contact angle θ corresponding to the equilibrium of the droplet. Now we make one of the main assumptions of our treatment: *we suppose that the boundary (the triple line) of the droplet is free to slip along the axis x*. It has to be emphasized that we solve the variational problem with *free endpoints* [11]. Thus, the conditions of transversality of the variational problem should be considered [11]. The transversality condition at the endpoint a yields:

$$(\tilde{G} - h'\tilde{G}'_{h'})_{x=a} = 0 \,, \quad (8)$$

where $\tilde{G}'_{h'}$ denotes the h' derivative of $\tilde{G}$ [11]. Substitution of Eq. (7) into the transversality condition, given by Eq. (8), and taking into account $h(a) = 0$, $U(x = a, h = 0) = 0$ will give rise to:

$$\left(\gamma\sqrt{1+h'^2} + \gamma_{SL} - \gamma_{SA} - \frac{\gamma h'^2}{\sqrt{1+h'^2}}\right)_{x=a} = 0 \,. \quad (9)$$

Simple transformations yield:

$$\left(\frac{1}{\sqrt{1+h'^2}}\right)_{x=a} = \frac{\gamma_{SA} - \gamma_{SL}}{\gamma} \,. \quad (10)$$

Considering $h'(x=a) = -\tan\theta_Y$, where θ_Y is the equilibrium (Young) contact angle immediately yields:

$$\cos\theta_Y = \frac{\gamma_{SA} - \gamma_{SL}}{\gamma} \,. \quad (11)$$

Equation 11 presents the well-known Young equation, illustrated with Fig. 3 (remarkably it could not be found in the famous essay by Thomas Young [13]). It asserts that the contact angle θ_Y is unambiguously defined by the triad of surface tensions: γ, γ_{SL}, γ_{SA}, as it was stated first verbally by Sir Thomas Young: "For each combination of

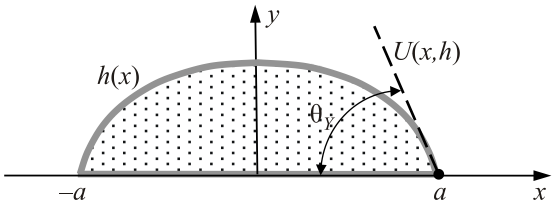

Fig. 2. A cross-section of the spherically-symmetrical droplet deposited on the ideal solid substrate and exposed to an external field $U(x,h)$.

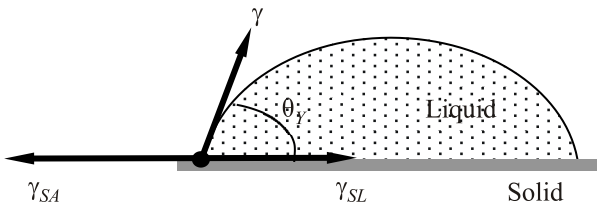

Fig. 3. Scheme illustrating the Young equation. The triad of surface tensions: γ, γ_{SL}, γ_{SA} may be interpreted as forces acting on the unit length of the triple (three-phase line).

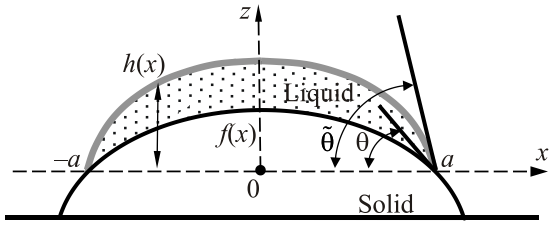

Fig. 4. Scheme of the section of a cylindrical drop deposited on a flat homogenous curved substrate.

a solid and a fluid, there is an appropriate angle of contact between the surfaces of the fluid, exposed to the air, and to the solid" [13]. The *Young contact angle* θ_Y is supplied by Eq. (11). The *Young contact angle* is the *equilibrium* contact angle that a liquid makes with an ideal solid surface [14]. It will be shown later that for droplets or surfaces with very small radii of curvature deposited on the *ideal* surfaces the equilibrium contact angle may be different due to line tension. Equation (11) tells us that the *Young angle* depends only on the physicochemical nature of the three phases and that it is *independent on the droplet shape and external field U* under very general assumptions about U, i.e., $U = U(x, h(x))$. The external field may deform the droplet but it has no influence on the Young angle θ_Y.

It should be emphasized that it is not simple to verify the Young equation experimentally, due to the fact that the solid/liquid interfacial tension is not well-measured physical value [10,12]. Moreover, the phenomenon of the contact angle hysteresis (see Sec. 3.1) complicates the experimental establishment of the Young (equilibrium) contact angle.

There also exist other simple ways of proving the Young equation by exploiting the principle of virtual works or other convenient methods of mathematical physics [15]. However, we preferred the variational approach for two reasons: 1) it demonstrated the independence of the equilibrium contact angle on the external fields (this fact is not so intuitively clear); 2) the variational approach will supply a key to much more complicated problems.

2.2. Wetting of flat homogeneous curved surfaces

Now consider wetting of flat homogeneous curved surfaces. For the sake of simplicity, we start with a 2D wetting problem where a cylindrical drop extended uniformly in the y direction is under discussion (Fig. 4 depicts the cross-section of such a drop). We consider the symmetrical about axis z liquid drop deposited on the curved solid substrate described by the given function $f(x)$ and exposed to some external field symmetric about axis z. The interaction of the droplet with the field gives rise to the linear energy density $U(x, h(x))$, as it was shown in the previous section. The free energy of the droplet is supplied by:

$$G(h,h') = \int_{-a}^{a} \left[\gamma\sqrt{1+h'^2} + (\gamma_{SL} - \gamma_{SA}) \times \right.$$

$$\left. \times \sqrt{1+f'^2} + U(x,h(x))\right] dx\,, \qquad (12)$$

where $h(x)$ is the local height of the liquid surface above the point x of the substrate (the profile of the droplet $h(x)$ is assumed to be a single-valued and even function). Condition of the constant area S has also to be taken into account:

$$S = \int_{-a}^{a} \left[h(x) - f(x)\right] dx = \text{const}\,. \qquad (13)$$

Note that this is equivalent to the constant volume requirement in the case of cylindrical "drops" (extended in the y direction; h is independent of y).

Equations (12), (13) reduce the problem to minimization of the functional:

$$G(h,h') = \int_{-a}^{a} \tilde{G}(h,h',x)dx\,, \qquad (14)$$

$$\tilde{G}(h,h',x) = \gamma\sqrt{1+h'^2} + (\gamma_{SL} - \gamma_{SA})\sqrt{1+f'^2} +$$

$$+ U(x,h) + \lambda(h-f)\,, \qquad (15)$$

where λ is the Lagrange multiplier to be deduced from Eq. (13). The constant terms in Eq. (15) could be omitted when the functional G is minimized; however, they turn out to be important for the analysis of the situation at the boundary. As mentioned above, we focus on the calculation of θ and ignore the calculation of the droplet's shape. As for flat surfaces the variational problem with *free endpoints* is solved; i.e., it is suggested now that the endpoints of the drop $x = \pm a$ are not fixed and are free to move along the line $f(x)$. Without the loss of generality, we suggest that the curve $f(x)$ and the entire problem are symmetrical around the vertical axis. Thus, the transversality condition in this case obtains the form [11]:

$$\left[\tilde{G} + G'_{h'}(f' - h')\right]_{x=a} = 0\,, \qquad (16)$$

where $\tilde{G}'_{h'}$ denotes the h' derivative of $\tilde{G}$. Substitution of Eq. (15) into the transversality condition, supplied by Eq. (16), and considering $h(a) = f(a)$, $U(a, h(a)) = 0$ gives rise to:

$$\left[\gamma\sqrt{1+h'^2} + (\gamma_{SL} - \gamma_{SA})\sqrt{1+f'^2} + \frac{\gamma h'(f'-h')}{\sqrt{1+h'^2}}\right]_{x=a} = 0. \quad (17)$$

Simple transformations yield:

$$\left[\gamma\frac{1+h'f'}{\sqrt{1+h'^2}} + (\gamma_{SL} - \gamma_{SA})\sqrt{1+f'^2}\right]_{x=a} = 0. \quad (18)$$

Considering $h'(x=a) = -\tan\theta$, where θ is the slope of the liquid-air interface at $x = a$, and $f'(x=a) = -\tan\tilde{\theta}$, where $-\tan\tilde{\theta}$ is the slope of the solid substrate in $x = a$, $(\tilde{\theta} < \pi/2)$ immediately gives:

$$\cos(\tilde{\theta} - \theta) = \frac{\gamma_{SA} - \gamma_{SL}}{\gamma}. \quad (19)$$

The Young equation (compare with Eq. (11)) is recognized. It is reasonable to define the equilibrium (Young) contact angle as $\tilde{\theta} - \theta$. The re-defined Young angle is insensitive to an external field, meeting the conditions: $U = U(x, h), U \neq U(h'), U(a, h(a)) = 0$.

Three dimensional flat homogeneous axially symmetrical surfaces are treated in a similar way. The free energy functional G supplying the free energy of the droplet assumes the form $G(h,h') = \int_0^a \tilde{G}(h,h',x)dx$, where:

$$\tilde{G}(h,h',x) = 2\pi\gamma x\sqrt{1+h'^2} + 2\pi x\sqrt{1+f'^2}(\gamma_{SL} - \gamma_{SA}) + \\ + U(x,h) + 2\pi\lambda x(h-f), \quad (20)$$

where λ is the Lagrange multiplier. The simple transformations akin to already presented result again in the Young equation for the 3D wetting of ideal surfaces [12].

2.3. Considering the line tension

Surface tension is due to the special energy state of the molecules at a solid or liquid surface [16]. Molecules located at the triple (three-phase) line where solid, liquid and gaseous phases meet are also in an unusual energy state. The notion of line tension has been introduced by Gibbs. Gibbs stated: "These (triple) lines might be treated in a manner entirely analogous to that in which we have treated surfaces of discontinuity. We might recognize linear densities of energy, of entropy, and of several substances which occur about the line, also a certain linear tension" [17]. In spite of the fact that the concept of line tension is intuitively clear, it remains one of the most obscure and disputable notions of the surface science [17]. The researchers disagree not only about the value of the line tension but even about its sign. Experimental values of a line tension Γ in the range of 10^{-5}–10^{-11} N were reported [10,12,16,17]. Very few methods allowing experimental measurement of line tension were developed [18–20]. Marmur estimated a line tension as $\Gamma \cong 4d_m\sqrt{\gamma_{SA}\gamma}\cot\theta_Y$, where d_m is the molecular dimension, γ_{SA}, γ are surface energies of solid and liquid correspondingly, and θ_Y is the Young angle. Marmur concluded that the magnitude of the line tension is less than $5\cdot10^{-9}$ N, and that it is positive for acute and negative for obtuse Young angles [21]. However, researchers reported negative values of the line tension for hydrophilic surfaces [19]. As to the magnitude of the line tension the values in the range 10^{-9}–10^{-12} N look realistic. Large values of Γ reported in the literature are most likely due to contaminations of the solid surfaces [10].

Let us estimate the characteristic length scale l at which the effect of line tension becomes important by equating surface and "line" energies: $l \cong \Gamma/\gamma = 1-100$ nm. It is clear that the effects related to line tension can be important for nano-scaled droplets or for nano-scaled rough surfaces [10,12].

Let us estimate the influence of the line tension on the contact angle of an axisymmetric droplet. The free energy functional supplying its free energy while also considering the line tension is given by: $G(h,h') = \int_0^a \tilde{G}(h,h',x)dx$, where:

$$\tilde{G}(h,h',x) = 2\pi\gamma x\sqrt{1+h'^2} + 2\pi x(\gamma_{SL} - \gamma_{SA}) + \\ + U(h,x) + 2\pi\lambda xh + 2\pi\Gamma. \quad (21)$$

For the sake of simplicity, Γ is anticipated as constant. Substitution of Eq. (21) into the transversality condition, defined by Eq. (8) yields:

$$\cos\theta = \frac{\gamma_{SA} - \gamma_{SL}}{\gamma} - \frac{\Gamma}{\gamma a}. \quad (22)$$

where a is the contact radius of the droplet [22]. Equation (22) represents the well-known Boruvka–Neumann formula considering the effect of line tension [17,22].

2.4. Very thin liquid films and the disjoining pressure

Consider very thin liquid films (typically with a thickness less than 10 nm) deposited on ideal solid surfaces. If we place a film of thickness e (see Fig. 5) on an ideal solid substrate its specific surface energy will be $\gamma_{SL} + \gamma$. However, if the thickness e tends to zero we return to a bare solid with a specific surface energy of γ_{SA} (see Refs. 10, 23,24). It is reasonable to present the specific surface energy of the film $\hat{G} = G/S$ (S is area) as:

$$\hat{G}(e) = \gamma_{SL} + \gamma + \Omega(e), \quad (23)$$

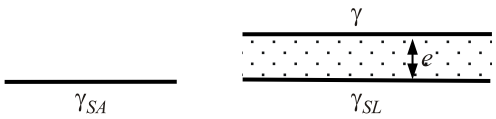

Fig. 5. Scheme illustrating the origination of the disjoining pressure. e is the thickness of a liquid film.

where $\Omega(e)$ is a function of the film defined in such a way that $\lim_{e\to\infty}\Omega(e)=0$ and $\lim_{e\to 0}\Omega(e)=\Psi=\gamma_{SA}-\gamma_{SL}-\gamma$ [10]. It could be shown that when the molecules of solid and liquid interact via the Van der Waals interaction (see Refs. 23,24), $\Omega(e)$ obtains the form:

$$\Omega(e)=\frac{A}{12\pi e^2}, \tag{24}$$

where A is the so called Hamaker constant, which is in the range of $A\cong 10^{-19}$–10^{-20} J [10,23,24]. The Hamaker constant could be expressed as:

$$A=\pi^2\bar{\omega}\tilde{\alpha}_L(\tilde{\alpha}_S-\tilde{\alpha}_L), \tag{25}$$

where $\tilde{\alpha}_L, \tilde{\alpha}_S$ are specific volume polarizabilities of liquid and solid substrate respectively, $\bar{\omega}$ is a constant that depends very little on the nature of solid and liquid [10].

It could be seen from Eq. (25) that the Hamaker constant could be positive or negative. It will be positive when the solid has higher polarizability than the liquid $(\tilde{\alpha}_S>\tilde{\alpha}_L)$. This situation can happen on high-energy surfaces; the opposite case occurs on low-energy surfaces $(\tilde{\alpha}_S<\tilde{\alpha}_L)$ [10]. It could be seen from Eq. (23) that, when $\Omega(e)<0$, it diminishes the specific surface energy of the solid/thin liquid film system thus the Van der Waals interaction will thin the film trying to cover as large a surface of the substrate as possible [10].

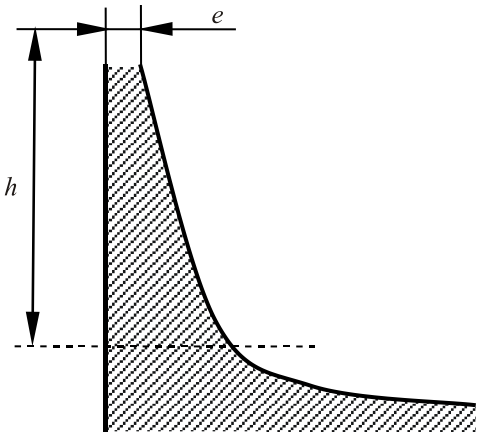

Fig. 6. Film of liquid helium climbing upwards due to the disjoining pressure.

The negative derivative of $\Omega(e)$ is called the disjoining pressure:

$$\Pi(e)=-\frac{d\Omega}{de}=\frac{A}{6\pi e^3}, \tag{26}$$

introduced into surface science by B.V. Derjaguin [25,26]. The disjoining pressure plays a primary role in the theory of thin liquid films deposited on solid surfaces, however one of the most amazing examples is discovered when liquid helium is deposited on a solid surface. The polarizability of liquid helium is lower than that of any solid substrate; thus the Hamaker constant given by Eq. (25) will be positive (this corresponds to the repulsive Van der Waals film force across an adsorbed helium film), and the disjoining pressure will thicken the film so as to lower its energy. Let us discuss the liquid helium film climbing a smooth vertical wall, depicted in Fig. 6, and derive the profile of the film $e(z)$. The components of the free energy of the unit area of the film depending on its thickness are supplied by:

$$\hat{G}(e)=\frac{A}{12\pi e^2}+\rho g h e. \tag{27}$$

The equilibrium corresponds to $\partial\hat{G}/\partial e=0$, which yields the thickness profile:

$$e(h)=\left(\frac{A}{6\pi\rho g h}\right)^{1/3}. \tag{28}$$

Considering the disjoining pressure becomes important for very thin angstrom-scaled films; however, when the liquid is water, the range of the effects promoted by the disjoining pressure could be as large as 100 Å, due to the Helmholtz charged double layer [10,23,24]. The electrical double layers give rise to the disjoining pressure described by an expression different from Eq. (26), i.e.

$$\Pi_{EDL}(e)=D\exp(-\chi e), \tag{29}$$

where $1/\chi\approx 100$ nm, and D is the characteristic parameter of the system, which can be either positive or negative [27]. Yet another component of the disjoining pressure Π_S is the so-called structural component caused by orientation of water molecules in the vicinity of the solid surface or at the aqueous solution/vapor interface [23,26]. Only a semi-empirical equation for the structural component of the disjoining pressure exists for today:

$$\Pi_S=\Lambda\exp(-\nu e), \tag{30}$$

where Λ and ν are constants, $1/\nu\approx 10$–15 Å [26,27].

2.5. Considering the influence of absorbed liquid layers and the liquid vapor

Up to this point we neglected two important factors: layers of absorbed liquid molecules which may be present on the solid substrate (still supposed to be ideal), and the impact of the gaseous phase. Consideration of these factors

was carried out recently by Starov and Velarde [27] They imposed three obvious conditions of the thermodynamic equilibrium of a droplet/substrate/vapor system. When the drop is in equilibrium, the chemical potentials of the liquid molecules in the ambient vapor phase and the liquid inside the droplet should be equal. The latter results in Kelvin's equation inside the drop:

$$p_L = \frac{RT}{V_{ML}} \ln \frac{p}{p_S}, \tag{31}$$

where $p_L = p_{\text{liq}} - p_{\text{vap}}$; $p_{\text{vap}}, p_{\text{liq}}$ are the pressures in the vapor and the liquid phases respectively, p_L is the Laplace pressure, V_{ML} is the molar volume of the liquid, p_S is the pressure of the saturated vapor at the temperature T above the flat liquid surface, R is the gas constant, and p is the vapor pressure, which is in equilibrium with the drop (for a detailed derivation and explanation of Kelvin's equation see Ref. 24). The Kelvin equation (Eq. (31)) was the first requirement of thermodynamic equilibrium, imposed on the problem of wetting of solid surface by a drop in Ref. 27.

Starov and Velarde also suggested that the solid substrate is covered by a thin layer of a thickness e of absorbed liquid molecules, as depicted in Fig. 7 [27]. The thermodynamic equilibrium requires equality of chemical potentials of molecules in the vapor phase and in the adsorbed layer. This was the second condition. And the third condition was a minimum of the excess free energy of a droplet. These conditions combined with use of the apparatus of transversality conditions of the variational problem of wetting leading to the following equation defining the contact angle θ:

$$\cos\theta \approx 1 + \frac{1}{\gamma}\int_e^\infty \Pi(e)de, \tag{32}$$

where $\Pi(e)$ is the disjoining pressure introduced in the previous paragraph. Emergence of $\Pi(e)$ in Eq. (32) predicting the contact angle is natural, the thickness of the adsorbed liquid layer is supposed to be nano-scaled [27]. It should be stressed that the contact angle θ needs redefinition, because the droplet cap does not touch the solid substrate, as shown in Fig. 7. Starov and Velarde defined the contact angle in this case as an angle between the horizontal axis and the tangent to the droplet cap profile at the point where it touches the absorbed layer of molecules (which is also called the *precursor film*) [27]. It is seen that Eq. (32) represents the obvious alternative to the Young Eq. (11), relating the Young angle to the disjoining pressure and not to the interplay of interfacial tensions.

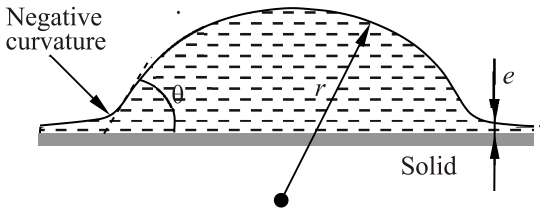

Fig. 7. Droplet of the radius r surrounded by the thin layer of liquid of the thickness e governed by the disjoining pressure.

Let us estimate the disjoining pressure in the absorbed layer according to $\Pi(e) = A/6\pi e^3$. If we will assume $A \approx 10^{-19}$–10^{-20} J, $e = 1$ nm we obtain giant values for the disjoining pressure: $\Pi(e) \cong 5\cdot 10^4$–$5\cdot 10^5$ Pa. For $e = 10$ nm we obtain much more reasonable values of the disjoining pressure: $\Pi(e) \cong 50$–$5\cdot 10^2$ Pa, however, they are still larger or comparable to the Laplace pressure in the drop. For $r \approx 1$ mm we have $p = 2\gamma/r \cong 140$ Pa. How is the mechanical equilibrium possible in this case? Perhaps it is due to the negative curvature of the droplet at the area where the cap touches the absorbed layer, shown in Fig. 7. Moreover, if we take for the disjoining pressure Eq. (26), we obtain from Eq. (32):

$$\cos\theta \approx 1 + \frac{1}{\gamma}\int_e^\infty \Pi(e)de = 1 + \frac{A}{12\pi\gamma e^2} > 1,$$

which corresponds to complete wetting [27]. The latter condition implies that at oversaturation no solution exists for an equilibrium liquid film thickness e outside the drop. If we take $A < 0$, there is a solution for an equilibrium liquid film thickness e but such an equilibrium state is unstable [27].

In order to understand how the partial wetting is possible in this case, Starov and Velarde discussed more complicated forms of disjoining pressure, comprising the London–van der Waals, double layer and structural contributions given by Eqs. (29), (30). They considered more complicated disjoining pressure isotherms, such as those depicted in Fig. 8 (curve *2*) [27]. The development of Eq. (32) yielded:

$$\cos\theta \approx 1 + \frac{1}{\gamma}\int_e^\infty \Pi(e)de \approx 1 - \frac{S_- - S_+}{\gamma}, \tag{33}$$

where S_- and S_+ are the areas depicted in Fig. 8. Obviously the partial wetting is possible when $S_- > S_+$ [27]. Thus, when a droplet is surrounded by a thin layer of liquid the possibility of partial wetting depends according to Starov and Velarde on the particular form of the Derjaguin isotherm [23].

2.6. Wetting transitions on ideal surfaces

The surface tension of liquids is temperature-sensitive; γ_{SA} and γ_{SL} are also temperature sensitive. What will be observed when both the droplet and substrate are heated? At a certain point, it may be that the sum of the solid-liquid and the liquid-air (vapor) surface tensions becomes equal to the solid–air (vapor) interfacial tension; then the spreading parameter $\Psi = \gamma_{SA} - (\gamma_{SL} + \gamma)$ will equal zero, and the transition from partial wetting to complete wetting will occur (see Fig. 1). The wetting transition is the transition

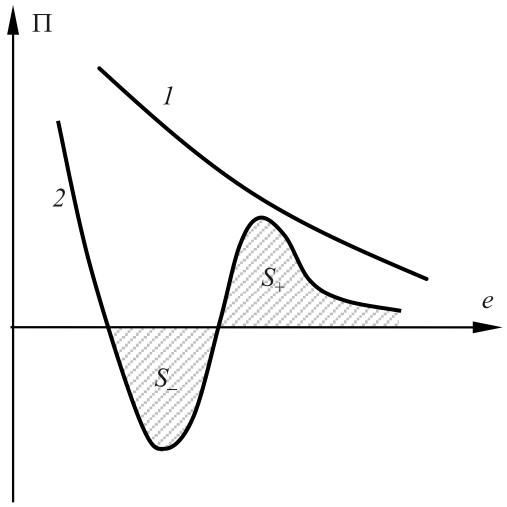

Fig. 8. Disjoining pressure (Derjaguin's isotherms): isotherm corresponding to the complete wetting, only the London–Van der Waals component is considered (*1*); isotherm comprising London, double layer and structural contributions and corresponding to the partial wetting (*2*).

between a partial and a complete wetting state [28]. The temperature of transition is called the *wetting temperature* T_W. The *order* of the wetting transition is determined — in the same manner as for a bulk phase transition — by the discontinuities of the surface free energy. If a discontinuity occurs in the first derivative of the free energy, the transition is said to be of the first order, and will take place in a discontinuous way. If the first derivative of the free energy is continuous at a phase transition point, then that indicates that it is a higher-order phase transition. For the wetting of a liquid drop on a substrate the relevant free energy is the surface tension of the substrate-air (vapor) interface γ_{SA}. Let us rewrite the Young equation in this a way:

$$\gamma_{SA} = (\gamma_{SL} + \gamma) - \gamma(1 - \cos\theta_Y). \qquad (34)$$

Since the term proportional to $\gamma(1-\cos\theta_Y)$ is the part that is going to zero at the wetting transition to complete wetting, it is the critical part of the specific free energy to be examined to determine the critical exponents. According to the definition of the critical exponent, this part of the specific free energy approaches zero following $(1-\cos\theta_Y) \infty (T_W - T)^{2-\hat{\alpha}}$, where $\hat{\alpha}$ is the specific heat exponent, determining the order of the wetting transition. For $\hat{\alpha} = 1$, the first derivative of $\cos\theta_Y$, and therefore the first derivative of the specific surface free energy is discontinuous with respect to temperature ($\cos\theta_Y = 1$, for $T \geq T_W$) and so the wetting transition is of the first order [28].

The accumulated experimental data and much theoretical work carried out in the field confirm the fact that wetting transitions are generally of the first order, as shown in Fig. 9. In this case, if one measures the thickness of the absorbed film beside the droplet, at the wetting transition a discontinuous jump in film thickness occurs from a microscopically thin to a thick film [28]. This is true for a broad range of liquid/solid pairs ranging from liquid helium to room temperature binary liquids and high temperature metallic systems. There were also several exceptions reported, for which a discontinuity in a higher derivative of the specific surface free energy was observed. Such a behavior was reported for liquid/air pairs governed by the long-range Van der Waals interactions [28].

3. Wetting of real surfaces

3.1. Contact angle hysteresis

The Young equation given by Eq. (11) predicts a sole value of the contact angle for a given ideal solid/liquid pair. As it always occurs in reality, however, the situation is much more complicated. Let us deposit a droplet onto an inclined plane, as described in Fig. 10 in the situation of partial wetting; it is latently supposed that the spreading parameter $\Psi < 0$. The inclined plane is supposed to be ideal, i.e. atomically flat, chemically homogeneous, isotropic, insoluble, non-reactive and non-deformed. We will nevertheless recognize different contact angles θ_1, θ_2, as shown in Fig. 10. This experimental observation definitely contradicts the predictions of the Young equation. Moreover, a droplet on an inclined plane could be in equilibrium only when contact angles θ_1, θ_2 are different [10,12]. If we increase the inclination angle α, contact angles θ_1, θ_2 will change, and at some critical angle α the droplet will start to slip. This critical contact angle is called the sliding angle. We conclude that a variety of contact angles can be observed for the same ideal solid substrate/liquid pair.

Let us perform one more simple experiment. When a droplet is inflated with a syringe as shown in Fig. 11 we observe the following picture: the triple line is pinned to

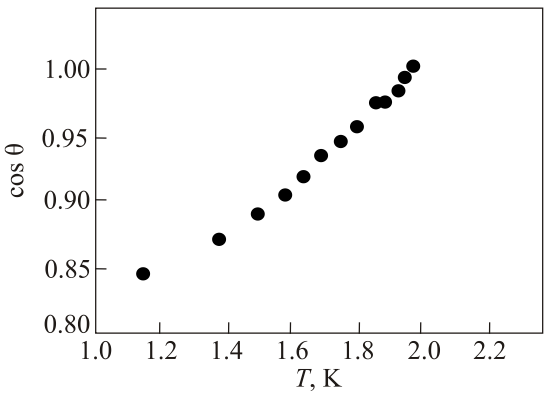

Fig. 9. Typical dependence of the cosine of the contact angle on the temperature, illustrating wetting transitions on flat substrates as established for liquid helium on cesium substrate; cosθ goes linearly to unity at the temperature of transition, indicating that the wetting transition is of the first order.

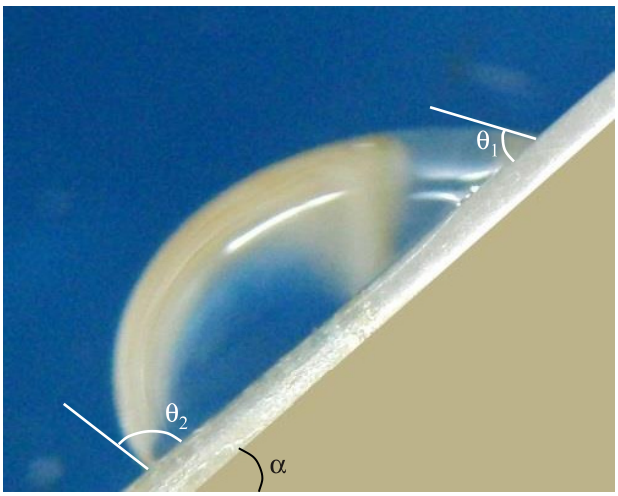

Fig. 10. (Color online) Drop on the inclined plane. Difference between contact angles θ_1, θ_2 prevents the droplet sliding; α is the inclination angle.

the substrate up to a certain volume of the droplet. When the triple line is pinned the contact angle increases till a certain threshold value θ_A beyond which the triple line does move. The contact angle θ_A is called the *advancing contact angle* [10,12]. When a droplet is deflated as depicted in Fig. 11, its volume can be decreased to a certain limiting value; in parallel the contact angle decreases till a threshold value θ_R, known as the *receding contact angle* [10,12]. When $\theta = \theta_R$, the triple line suddenly moves. Both θ_A and θ_R are equilibrium, although metastable contact angles [10,12]. The difference between θ_A and θ_R is called the *contact angle hysteresis*.

Both measurement and understanding of the phenomenon of the contact angle hysteresis remain challenging experimental and theoretical tasks. It is customary to attribute the phenomenon of the contact angle hysteresis to physical or chemical heterogeneities of the substrate [10,12]; however, even ideal substrates discussed in the previous Sections demonstrate significant contact angle hysteresis. We'll start our discussion from the physical reasons of the contact angle hysteresis on ideal substrates.

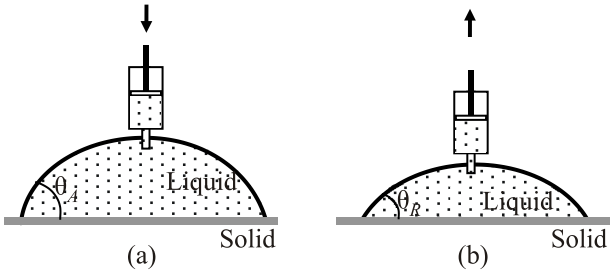

Fig. 11. Inflating and deflating of a droplet. Advancing θ_A and receding contact angles θ_R are shown.

3.2. Contact angle hysteresis on smooth homogeneous substrates

Contact angle hysteresis has been registered even for silicon wafers which are regarded as atomically flat rigid substrates, and are considered very close to be ideal ones. Extrand et al. studied the contact angle hysteresis for various liquids, including water, ethylene glycol, methylene iodide, acetophenone and formamide, deposited on silicon wafers with a tilted plane method [29]. Contact angle hysteresis (defined as $\theta_A - \theta_R$) as high as 14° was established for the water/silicon wafer and methylene iodide/silicon wafer pairs. It should be mentioned that the contact angle hysteresis on the order of magnitude of 5–10° has been reported for other silicon wafer/liquid pairs [29]. High contact angle hysteresis has been observed also for atomically smooth polymer substrates. Lam *et al*. used polymer-coated silicon wafers for study of the contact angle hysteresis, and reported the values of contact angle hysteresis on the order of tens of degrees [30] The question is: how is such dispersion of contact angles possible, in contradiction to the predictions of the Young equation?

The explanation of the contact angle hysteresis observed on smooth surfaces becomes possible if we consider the effect of the *pinning of the triple line*. The intermolecular forces acting between molecules of solid and those of liquid, which pin the triple line to the substrate, are responsible for the contact angle hysteresis. Yaminsky developed an extremely useful analogy between the phenomena occurring at the triple line with the static friction [31]. I quote: "… for a droplet on a solid surface there is a static resistance to shear. It occurs *not over the entire solid-liquid interface, but only at the three-phase line*…". This paradox is easily resolved once one realizes that the liquid–solid interaction is in fact not involved in the process of overflow of liquids above solid surfaces. A boundary condition of zero shear velocity typically occurs even for liquid-liquid contacts… But even given that the strong binding condition does apply to solid–liquid interfaces, this does not prevent the upper layer of the liquid from flowing above the "stagnant layer" of a gradient velocity. The movement of the liquid over the wetted areas occurs in the absence of static resistance. Interaction in a manner of dry friction occurs only at the three-phase line [31].

Thus, the contact angle hysteresis on ideal surfaces is caused by the intermolecular interaction between molecules constituting a solid substrate and a liquid; this interaction pins the triple line and gives rise to a diversity of experimentally observed contact angles [30,31].

3.3. Contact angle hysteresis on real surfaces

Real surfaces are rough and chemically heterogeneous. The macroscopic parameter describing wetting of surfaces is the *apparent contact angle* [14]. The apparent contact angle is an equilibrium contact angle measured macroscop-

ically on a solid surface that may be rough or chemically heterogeneous [10,12,14]. The detailed microscopic topography of a rough or chemically heterogeneous surface cannot be viewed with regular optical means; therefore this contact angle is defined as the angle between the tangent to the liquid-vapor interface and the apparent solid surface as macroscopically observed [10,12,14]. Actually the spectrum of apparent contact angles is observed on real surfaces. A diversity of physical factors contributes to the contact angle hysteresis, including the pinning of the triple line, liquid penetration and surface swelling, deformation of the substrate, etc [12,30]. It should be emphasized that the contact angle hysteresis turned out to be a complicated, time-dependent effect. The contact angle hysteresis, as it seen from the phenomenological point of view, is due to the multiple minima of the free energy of a droplet deposited on the substrate. These minima are separated by potential barriers [32]. Contact angle hysteresis is strengthened by the roughness and chemical heterogeneity of a substrate [33]. The comprehensive review of the contact angle hysteresis is supplied in Refs. 10,12.

3.4. Deformation of the substrate as an additional source of the contact angle hysteresis

Let us take a closer look at the Young Eq. (11) and Fig. 3. The Young equation could be interpreted as the balance of horizontal projections of forces acting on the triple line. However, the vertical balance is still neglected. The component of the liquid surface tension $\gamma \sin\theta$ perpendicular to the plane of the solid (see Fig. 12) must be equilibrated, and this leads necessarily to some distortion of the substrate near the triple line, called the "wetting ridge" [34,35]. This distortion is negligible for rigid substrates such as glass or steel, but it should be considered for soft substrates such as rubbers (elastomers) [36]. This wetting ridge (depicted in Fig. 12) leads to additional pinning of the triple line and strengthens the contact angle hysteresis.

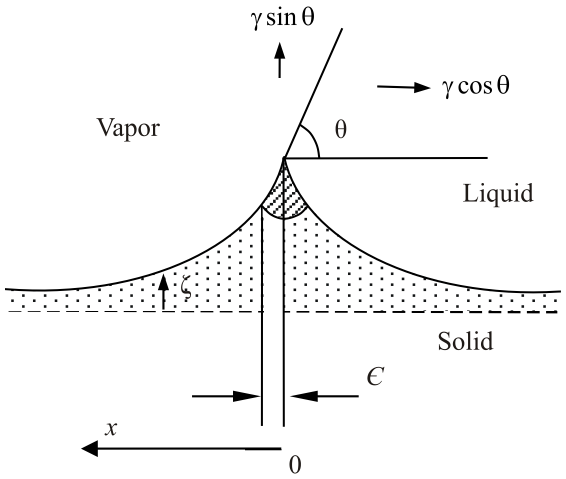

Fig. 12. Scheme of the wetting ridge. ζ is the vertical displacement caused by the vertical component of surface tension $\gamma \sin\theta$. ϵ is the cutoff distance for linear elastic behavior.

The problem of elastic deformation of a substrate by a droplet was treated in Refs. 34–36. The scaling dimensionless parameter δ, relating contributions of surface tension and elastic terms, could be introduced according to:

$$\delta = \frac{\gamma_{SA}}{\mu d}, \tag{35}$$

where μ is the elastic (shear) modulus of the solid, and d is the depth (thickness of the substrate) [34–36]. For distances much larger than the thickness d the vertical displacement ζ (see Fig. 12) decays exponentially:

$$\zeta \cong \frac{\gamma \sin\theta}{\mu} \sin\frac{|x|}{\kappa} \exp\left(-\frac{|x|}{k'}\right), \tag{36}$$

where x is a distance measured from the triple line parallel to the undisturbed surface (see Fig. 12), and κ, k' are characteristic lengths of the order d [34]. At intermediate distances $\delta d < x < d$ the deformation ζ is given by:

$$\zeta \cong \frac{\gamma \sin\theta}{2\pi\mu} \ln\frac{d}{|x|}. \tag{37}$$

Equation 37 is true for $|x| > \epsilon$, where ϵ is a cutoff length, below which the solid no longer behaves in a linearly elastic manner (typically on the order of a few nanometers for an elastomer) [34–36]. At short distances $(x < \delta d)$ the vertical displacement ζ is estimated as:

$$\zeta \cong \frac{1}{2\pi} \frac{\gamma \sin\theta}{\mu} \ln\frac{1}{\delta}. \tag{38}$$

For the details of the solution of a problem of distortion of a soft substrate by a droplet see Ref. 34–36. Anyway, this distortion is not negligible for soft materials such as elastomers and it contributes essentially to the contact angle hysteresis.

3.5. The dynamic contact angle

Until this Section we have discussed only the statics of wetting. Now we'll consider a much more complicated situation: when the triple line moves. When the triple line moves the dynamic contact angle θ_D does not equal the Young angle as shown in Fig. 13. It may be larger or smaller than the Young angle (see Fig. 13). The excess force pulling the triple line is given by (see Ref. 10):

$$F(\theta_D) = \gamma_{SA} - \gamma_{SL} - \gamma \cos\theta_D. \tag{39}$$

As we already mentioned in the previous section the effect of contact angle hysteresis complicates the study of wetting even in a static situation. The movement of the triple line introduces additional difficulties, so the reproducibility of the results of the measurements of dynamic contact an-

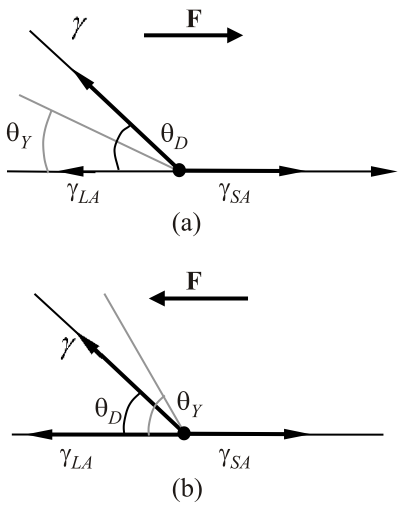

Fig. 13. Origin of the dynamic contact angle θ_D. The dynamic contact angle θ_D is larger than the Young angle θ_Y (a). The opposite situation: the dynamic contact angle θ_D is smaller than the Young angle θ_Y (b).

gles becomes a challenging task [10]. We'll start from the theoretical analysis of dynamic wetting on ideally smooth, rigid, non-reactive surfaces.

Now we find ourselves in the realm of hydrodynamics. Systematic study of the problem of the dynamics of wetting has been undertaken by Voinov [37]. When the inertia-related contributions are neglected (and this is the case in the model proposed by Voinov) the only dimensionless number, governing the flow is the *capillary number Ca*, defined as:

$$Ca = \frac{\eta v}{\gamma}, \tag{40}$$

where v is the characteristic velocity and η is the viscosity of the liquid. The capillary number describes the interplay between the viscosity and surface tension induced effects. Voinov also phenomenologically introduced the angle of the free surface slope θ_m at the height of the limiting scale h_m:

$$\theta_D = \theta_m, \quad h = h_m. \tag{41}$$

Voinov noted that θ_m is unknown beforehand and should be determined during the solution of the problem [37]. The accurate mathematical solution of the hydrodynamic problem of wetting yielded for the dynamic contact angle:

$$\theta_D(h) = \left[\theta_m^3 + 9\frac{\eta v}{\gamma}\ln\frac{h}{h_m}\right]^{1/3} = \left[\theta_m^3 + 9Ca\ln\frac{h}{h_m}\right]^{1/3}. \tag{42}$$

Equation (42) is referred as the Cox–Voinov law, and it is valid for $\theta_D < 3\pi/4$ (see Ref. 37). Hoffmann has shown that the experimental dependence $\theta_D(Ca)$ is represented by a universal curve (corrected with a shifting factor) for a diversity of liquids [38]. A detailed discussion of the validity and applicability of the Cox–Voinov law is supplied in Ref. 39. It is seen from Eq. (42) that the slope varies logarithmically with the distance from the triple line. Thus, it is impossible to assign a unique dynamic contact angle to a triple line moving with a given speed [39]. Hence, Fig. 13 depicts an obvious oversimplification of the actual dynamic wetting situation. It is also noteworthy that θ_D depends slightly on the cut-off length h_m, however, it depends strongly on the microscopic angle θ_m. For a detailed discussion of actual values of θ_m and h_m, see Ref. 39.

3.6. Wetting of rough and chemically heterogeneous surfaces: the Wenzel and Cassie models

In this Section present models describing the wetting of rough and chemically heterogeneous surfaces, i.e., the Wenzel and Cassie models. Recall that wetting of rough or chemically heterogeneous surfaces is characterized *by the apparent contact angle*, introduced in the Sec. 3.3. The Cassie and Wenzel models predict the apparent contact angle, which is an essentially macroscopic parameter. This fact limits the field of validity of these models: they work when the characteristic size of a droplet is much larger than that of the surface heterogeneity or roughness. The use of the Wenzel and Cassie equations needs a certain measure of care; numerous misinterpretations of these models are found in the literature.

Let us start from the Wenzel model, introduced in 1936, which deals with the wetting of rough, chemically homogeneous surfaces and implies total penetration of a liquid into the surface grooves, as shown in Fig. 14 [40,41]. When the spreading parameter $\Psi < 0$ (see Sec. 2.1 and Fig. 1(a)), a droplet forms a cap resting on the substrate with an apparent contact angle θ^*. If the axisymmetric droplet is exposed to an external field $U(x,h)$, the free energy of G could be written as:

$$G(h,h') = \int_o^a \left[2\pi\gamma x\sqrt{1+h'^2} + 2\pi x(\gamma_{SL} - \gamma_{SA})\tilde{r} + U(x,h)\right]dx, \tag{43}$$

where $h(x,y)$ is the local height of the liquid surface above the point (x,y) of the substrate, $U(x,h(x))$ is the linear density

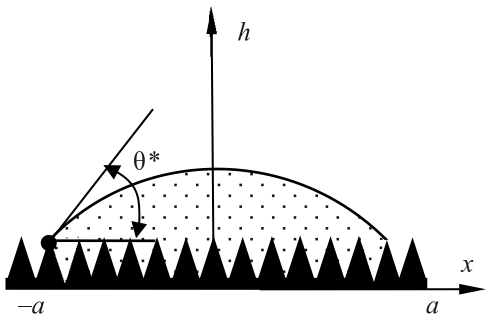

Fig. 14. Wenzel wetting of a chemically homogeneous rough surface: liquid completely wets the grooves. θ^* is the apparent contact angle.

of interaction of the droplet with the external field with the dimension of J/m, a is the contact radius, and the integral is extended over the substrate area (see Sec. 2.1). Equation (43) is very similar to Eq. (4), the only difference being parameter $\tilde{r}$ which is the roughness ratio of the wet area; in other words, the ratio of the real surface in contact with liquid to its projection onto the horizontal plane. Parameter $\tilde{r}$ describes the increase of the wetted surface due to roughness, and obviously $\tilde{r} > 1$ takes place. We also suppose that the volume of a droplet is constant (see Eq. (5)). Equations (5), (43) reduce the problem to the minimization of the functional:

$$G(h,h') = \int_0^a \tilde{G}(h,h',x)dx\,, \tag{44}$$

where:

$$\tilde{G}(h,h',x) = 2\pi\gamma x\sqrt{1+h'^2} + 2\pi x(\gamma_{SL} - \gamma_{SA})\tilde{r} + \\ + U(x,h) + 2\pi\lambda xh\,, \tag{45}$$

where λ is the Lagrange multiplier to be deduced from Eq. (5).

The use of the conditions of transversality of the variational problem, akin to that, presented in detail in Sec. 2.1 yields:

$$\cos\theta^* = \tilde{r}\cos\theta_Y\,. \tag{46}$$

Equation (46) presents the famous Wenzel equation [40,41]. Three important conclusions follow from Eq. (46):

—Inherently smooth hydrophilic surfaces $(\theta_Y < \pi/2)$ will be more hydrophilic when riffled: $\theta^* < \theta_Y$ due to the fact, that $\tilde{r} > 1$.

—Due to the same reason, inherently hydrophobic flat surfaces $(\theta_Y < \pi/2)$ will be more hydrophobic when grooved: $\theta^* > \theta_Y$.

—The Wenzel apparent contact angle, given by Eq. (46), *is independent on the droplet shape and external field U* under very general assumptions about U, i.e., $U = U(x, h(x))$.

Wenzel wetting of chemically homogeneous curved rough surfaces is discussed in Ref. 42.

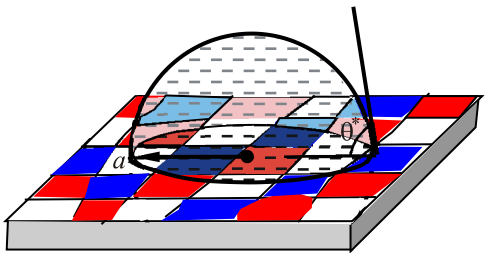

Fig. 15. (Color online) Cassie–Baxter wetting of flat chemically heterogeneous surfaces (various colors correspond to different chemical species). θ^* is the apparent contact angle.

The Cassie–Baxter wetting model, introduced in Refs. 43,44, deals with the wetting of flat chemically heterogeneous surfaces. Suppose that the surface under the drop is flat, but consists of n sorts of materials randomly distributed over the substrate as shown in Fig. 15. This corresponds to the assumptions of the Cassie–Baxter wetting model [43,44]. Each material is characterized by its own surface tension coefficients $\gamma_{i,SL}$ and $\gamma_{i,SA}$, and by the fraction f_i in the substrate surface, $f_1 + f_2 + \ldots + f_n = 1$. The free energy of an axisymmetric drop of a radius a exposed to an external field $U(x, h)$ will be given by the following expression (analogous to Exp. (5.1)):

$$G(h,h') = \int_o^a \Big[2\pi\gamma x\sqrt{1+h'^2} + \\ + 2\pi x\sum_{i=1}^n f_i(\gamma_{i,SL} - \gamma_{i,SA}) + U(x,h)\,dx\,. \tag{47}$$

Equation (5), demanding the constancy of the droplet volume, again introduces the Lagrange multiplier λ. Analogously to the above treatment we obtain for $\tilde{G}$:

$$\tilde{G}(h,h',x) = 2\pi\gamma x\sqrt{1+h'^2} + 2\pi x\sum_{i=1}^n f_i(\gamma_{i,SL} - \gamma_{i,SA}) + \\ + U(x,h) + 2\pi\lambda xh\,. \tag{48}$$

Substitution of Exp. (48) into the transversality condition, given by Eq. (8) and transformations akin to aforementioned ones yield the famous Cassie–Baxter equation:

$$\cos\theta^* = \frac{\sum_{i=1}^n f_i(\gamma_{i,SA} - \gamma_{i,SL})}{\gamma}\,, \tag{49}$$

predicting the so-called Cassie apparent contact angle θ^* on flat chemically heterogeneous surfaces [12,43,44]. We demonstrated convincingly that the Cassie apparent contact angles are also insensitive to external fields [12,22]. When the substrate consists of two kinds of species, the Cassie–Baxter equation obtains the form:

$$\cos\theta^* = f_1\cos\theta_1 + f_2\cos\theta_2\,, \tag{50}$$

which is widespread in the scientific literature dealing with the wetting of heterogeneous surfaces [10,12,24,43,44]. The presented derivation demonstrates explicitly that the Cassie–Baxter apparent contact angle is insensitive to external fields of a very general form, i.e., $U = U(x, h(x))$.

The peculiar form of the Cassie–Baxter equation, given by Eq. (50), was successfully used for the explaining the phenomenon of superhydrophobicity, which will be discussed in detail in the next Section. Jumping ahead, we admit that in the superhydrophobic situation, a droplet is partially supported by solid substrate and partially by air cushions, as shown in Fig. 16. Consider a situation where

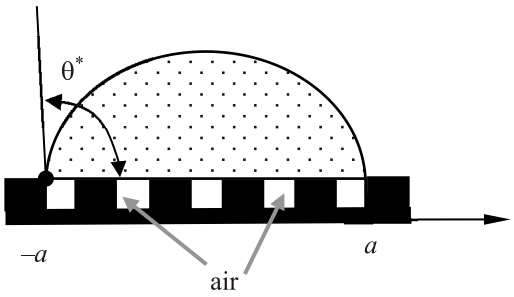

Fig. 16. The particular case of the Cassie wetting: a droplet is partially supported by solid and partially by air cushions. θ^* is the apparent contact angle.

the mixed surface is comprised of solid surface and air pockets, with the contact angles θ_Y (which is the Young angle of the solid substrate) and π respectively. We denote by f_s and $1-f_S$ relative fractions of solid and air respectively. Thus, we deduce from Eq. (50):

$$\cos\theta^* = -1 + f_S(\cos\theta_Y + 1)\,. \qquad (51)$$

As it always takes place in nature, the pure Wenzel and Cassie wetting regimes introduced in previous Sections are rare in occurrence. More abundant is a so-called mixed wetting state, depicted schematically in Fig. 17, introduced in Ref. 45 and discussed in much detail in Ref. 46 In this situation the use of transversality conditions of the variational problem of wetting yields for the apparent contact angle:

$$\cos\theta^* = \tilde{r} f_S \cos\theta_Y + f_S - 1\,. \qquad (52)$$

Obviously for $\tilde{r} = 1$, we return to the usual Cassie air-trapping described by Eq. (51). Equation (52) is extremely useful for understanding the phenomenon of superhydrophobicity to be discussed in detail in the next Section. For considering the role of line tension in wetting of chemically heterogeneous surfaces see Refs. 47,48.

4. Superhydrophobicity and the rose petal effect

4.1. Superhydrophobicity

The phenomenon of superhydrophobicity was revealed in 1997, when W. Barthlott and C. Neinhuis studied the wetting properties of a number of plants and stated that the

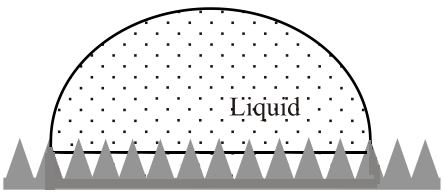

Fig. 17. The mixed wetting state. The droplet is partially supported by the solid and partially by air cushions.

"interdependence between surface roughness, reduced particle adhesion and water repellency is the keystone in the self-cleaning mechanism of many biological surfaces" [9]. They discovered the extreme water repellency and unusual self-cleaning properties of the "sacred lotus" (*Nelumbo nucifera*) and coined the notion of the "lotus effect", which is now one of the most studied phenomena in surface science. Afterwards, the group led by W. Barthlott studied a diversity of plants and revealed a deep correlation between the surface roughness of plants, their surface composition and their wetting properties (varying from superhydrophobicity to superhydrophilicity) [49–51].

The amazing diversity of the surface reliefs of plants observed in nature was reviewed in Ref. 49. Barthlott *et al*. also clearly understood that the micro- and nano-structures of the plants surfaces define their eventual wetting properties, in accordance with the Cassie–Baxter and Wenzel models (discussed in detail in the previous Section) [49–51]. Since Barthlott *et al*. reported the extreme water repellency of the lotus, similar phenomena were reported for a diversity of biological objects: water strider legs, as well as bird and butterfly wings [52–55].

All the phenomenon was called superhydrophobicity and natural and artificial surfaces characterized by an apparent contact angle larger than 150° are referred to as superhydrophobic [9,10,52–55]. It should be emphasized that high apparent contact angles observed on a surface are not sufficient for referring it as superhydrophobic [56–58]. True superhydrophobicity should be distinguished from the pseudo-superhydrophobicity inherent to surfaces exhibiting the "rose petal effect" to be discussed later. The pseudo-superhydrophobic surfaces are characterized by large apparent contact angles accompanied by the high contact angle hysteresis. In contrast, truly superhydrophobic surfaces are characterized by large apparent contact angles and low contact angle hysteresis resulting in a low value of a sliding angle: a water drop rolls along such a surface even when it is tilted at a small angle. Truly superhydrophobic surfaces are also self-cleaning, since rolling water drops wash off contaminations and particles such as dust or dirt. Actually, the surface should satisfy one more demand to be referred as superhydrophobic: the Cassie–Baxter wetting regime on this surface should be stable [59].

The Cassie–Baxter equation (Eq. (51)), developed for the air trapping situation where the droplet is partially supported by air cushions (see Fig. 16), supplies the natural explanation for the phenomenon of superhydrophobicity. Indeed, the apparent contact angle θ^* in this situation given by: $\cos\theta^* = -1 + f_S(\cos\theta_Y + 1)$ ultimately approaches π when the relative fraction of the solid f_s approaches zero. This corresponds to complete dewetting, discussed in the Sec. 2.1 and illustrated by Fig. 1(c). Note that the apparent contact angle also approaches π when the Young angle tends to π. However, this situation is practically unachievable, because the most hydrophobic polymer, polytetra-

fluoroethylene (Teflon) demonstrates an advancing angle smaller than 120°, and this angle is always larger than the Young one. Hence, it is seen from the Cassie–Baxter equation that the apparent contact angles could be increased by decreasing the relative fraction of the solid surface underneath a droplet. However, there exists a more elegant way to manufacture surfaces characterized by ultimately high apparent contact angles: producing hierarchical reliefs [12,59,60], and this is the situation observed in natural objects such as lotus leaves and birds' wings [9,55].

Note, that the Wenzel equation (Eq. (46)) also predicts high apparent contact angles approaching π for inherently hydrophobic surfaces ($\theta_Y > \pi/2$), when $\tilde{r} >> 1$. However, the Wenzel-like wetting, depicted in Fig. 14, is characterized by the high contact angle hysteresis, whereas superhydrophobicity accompanied by self-cleaning calls for the contact angle hysteresis to be as low as possible.

4.2. Wetting of hierarchical reliefs: approach of Herminghaus

Herminghaus developed a very general approach to the wetting of hierarchical reliefs, based on the concept of the effective surface tension of a rough solid/liquid interface γ_{SL}^{eff} [61]. It is reasonable to suggest phenomenologically that this surface tension is increased when compared to that of the flat solid surface γ_{SL}, due to the roughness. Herminghaus treated indented surfaces; however, his approach keeps its validity for bumpy ones as well. The effective surface tension of a rough surface with a single-scale roughness is given by:

$$\gamma_{SL1}^{\text{eff}} \cong (1 - f_L)\gamma_{SL} + f_L(\gamma + g_0\gamma_{SA}), \qquad (53)$$

where f_L is the fraction of free liquid surfaces suspended over the indentations of the relief, $g_0 \geq 1$ is the geometrical factor describing the total surface area of the indentation, γ_{SA} is the surface tension of the flat solid surface/air interface, and the subscript 1 in $\gamma_{SL1}^{\text{eff}}$ denotes the single-scale type of the roughness. It is seen from Eq. (53) that an indented interface has a larger effective surface tension than a flat one. This warrants the apparent contact angle θ_1 larger than θ_Y inherent to the flat surface, but does not explain the exceptionally large apparent contact angles observed on many biological objects [52–55]. In order to explain the extreme apparent contact angles Herminghaus analyzed hierarchical reliefs, such as those depicted in Fig. 18. For such a double-scaled relief, the effective surface tension will be given by:

$$\gamma_{SL2}^{\text{eff}} \cong (1 - f_{L1})\gamma_{SL1} + f_{L1}(\gamma + g_1\gamma_{SA}(1 + (g_0 - 1)f_L)). \qquad (54)$$

For hierarchically indented substrates, Herminghaus deduced the following recursion relation:

$$\cos\theta_{n+1} = (1 - f_{Ln})\cos\theta_n - f_{Ln}, \qquad (55)$$

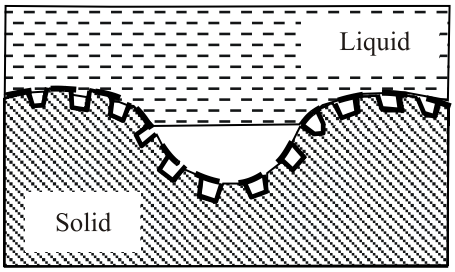

Fig. 18. Scheme of wetting of a hierarchical relief (for details see Ref. 61).

where n denotes the number of the generation of the indentation hierarchy. A larger n corresponds to a larger length scale. According to Eq. (55), $\cos\theta_{n+1} - \cos\theta_n = -f_{Ln}(1 + \cos\theta_n) < 0$, so that the sequence represented by Eq. (55) is monotonic. Herminghaus stressed that θ_0 corresponding to θ_Y must only be finite, but need not exceed $\pi/2$ for obtaining high resulting apparent contact angles on hierarchical surfaces. Herminghaus also considered fractal surfaces and estimated the Hausdorf dimension of such surfaces. Generally, the model proposed by Herminghaus successfully explained high apparent contact angles observed on a diversity of biological objects [52–55].

It is noteworthy, that hierarchical surfaces enable design of superoleophobic surfaces (depicted in Fig. 19), which repel no only water but also organic oils, which is an important technological task [62–65].

4.3. The rose petal effect

It was already mentioned in the Sec. 4.1 that high apparent contact angles are necessary but not sufficient for true superhydrophobicity accompanied by self-cleaning properties of a surface. Low contact angle hysteresis and high stability of the Cassie wetting states are also necessary (the problem of the stability of the Cassie wetting state was studied recently in detail in Refs. 66–71).

Jiang *et al*. reported that rose petal surfaces demonstrate high contact angles attended with extremely high contact angles hysteresis [72]. The surface of the rose petal is built from hierarchically riffled "micro-bumps" resembling those of lotus leaves [9,72]. At the same time, the wetting of rose petals is very different from that of lotus leaves. The apparent angles of droplets placed on a rose petal are high, but the droplets are simultaneously in a "sticky" wetting state; they do not roll or slip, when put on an inclined plane (it seems that the first systematic treatment of the physics of droplets, placed on inclined planes was carried out by the distinguished physicist Yakov Ilyitch Frenkel in Ref. 73; restoring historical justice calls for mentioning that Frenkel first clearly demonstrated that the Young equation is actually the boundary condition of the problem of wetting (see also Secs. 2.1, 2.2, and 3.6). Water droplets on rose petals kept the spherical shape and did not slide

even when the surface was turned upside down, Jiang called this phenomenon the "rose petal effect" [72].

Later, very similar wetting behavior was revealed on surfaces built from *lycopodium particles* [74]. Lycopodium particles, which are spores of the plant *Lycopodium clavatum*, are microscopically scaled porous balls with the external diameter of 20–30 μm, and they are characterized by a pronounced hierarchical structure [74]. Lycopodium particles comprise pores with a characteristic size of 3–5 μm, thus according to the approach developed in the Sec. 4.2, these particles are well expected to exemplify pronounced superhydrophobicity. Indeed, surfaces built from these particles demonstrate apparent contact angles as high as 150° [74]. However, droplets deposited on these surfaces did not slide when the surface was tilted; moreover, they were steadily attached even when the surface was turned upside down, as shown in Ref. 74. Artificial surfaces demonstrating the "rose petal effect" have been also reported [75].

The natural explanation for the "rose petal effect" is supplied by the Wenzel model (see Sec. 3.6). Inherently hydrophobic flat surfaces may demonstrate apparent contact angles approaching π when rough [76]. Wenzel wetting is characterized by the high contact angle hysteresis. However, the Wenzel model does not explain the existence of the "rose petal effect" for inherently hydrophilic surfaces. Bhushan and Nosonovsky demonstrated that wetting of hierarchical reliefs may be of a complicated nature, resulting in the "rose petal effect", as shown in Fig. 20 [77]. Various wetting modes are possible for hierarchical reliefs: it is possible that a liquid fills the larger grooves, whereas small-scaled grooves are not wetted and trap air as shown in Fig. 20(a). The inverse situation is also possible, in which small-scaled grooves are wetted and large scale ones form air cushions (see Fig. 20(b)). According to Ref. 77

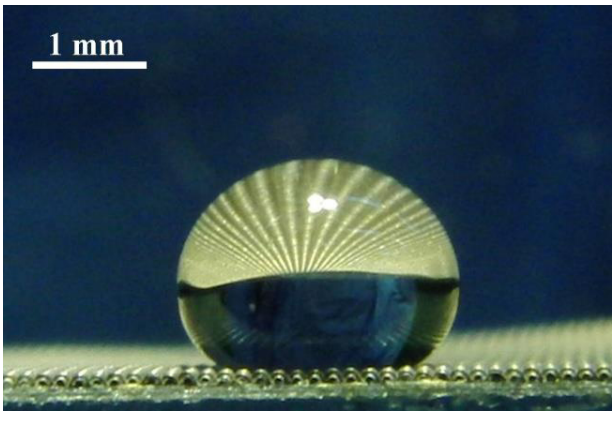

Fig. 19. (Color online) The phenomenon of superoleophobicity. Castor-oil droplet with a volume of 8μL placed on the superoleophobic surface. High apparent contact angle is clearly seen. The image is taken in the Laboratory of Polymers of the Ariel University.

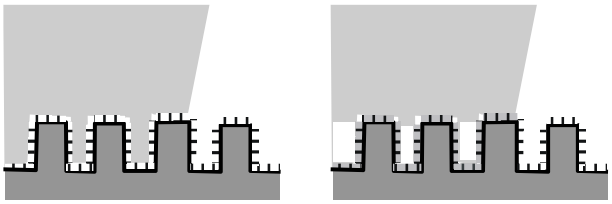

Fig. 20. Schemes of various wetting scenarios possible on a hierarchical relief (for details see Ref. 77).

the larger structure controls the contact angle hysteresis, whereas the smaller (usually nanometric) scale is responsible for high contact angles [77,78]. Thus, the relief depicted in Fig. 20(a) will demonstrate high contact angles attended by high contact angle hysteresis. This hypothesis reasonably explains the "rose petal effect" [77]. However, it is clearly seen that a broad variety of wetting modes is possible on hierarchical surfaces [77,78]. When the smaller scale is nanometrically scaled the effects due to the disjoining pressure (see Sec. 2.4) are already non-negligible.

It should be stressed that various stimuli such as pressure, temperature or external fields may promote the transition from the low friction Cassie wetting state to the sticky Wenzel state, which are usually separated by the potential barrier [66–70]. The physics of these so called Cassie-Wenzel transitions is reviewed in Ref. 71.

4.4. Wetting phenomena and molecular dynamic simulations

Till now, we kept pure a macroscopic approach. New insights came to the physics of wetting from computer simulations, recently reported by several groups for study of capillarity; in particular computer simulations are useful for study of the stability of the Cassie-like wetting [66,71,79–81]. Savoy *et al.* calculated the energy barriers separating the Cassie and Wenzel states [82,83]. It is well accepted that for macroscopic droplets, the energetic barrier separating the Cassie state and Wenzel state is extremely large compared to thermal fluctuations. However, it was shown with molecular simulations for nano-droplets that this barrier becomes comparable to the energy of thermal fluctuations and ranges from $8k_BT$ to a few tenths of k_BT [84].

5. Summary

Wetting phenomena starting from Plinius the elder via B. Franklin, Th. Young, W. Thomson and Lord Rayleigh in the epoch of the classical physics and afterwards via Einstein, Shrödinger, Bohr and de Gennes in the realm of modern physics are continuing to inspire fascinating experimental and theoretical studies.These effects are important from both fundamental and applicative points of view while governing spreading of liquids on natural and artifi-

cial surfaces, numerous biological events and technological processes such as painting, printing and gluing. The review presents the general physical approach to capillarity effects, based on the variational treatment of the appropriate problem of wetting. It is demonstrated that basic equations describing wetting of ideal and real (rough and chemically heterogeneous) surfaces, namely the Young, Wenzel and Cassie–Baxter equations, arise at the transversality conditions of variational problems of wetting, which are defined as "problems with free endpoints". Thus, general thermodynamic approach to the effects occurring at solid/liquid interfaces becomes possible. The low temperature wetting events, such as wetting transitions and spreading of liquid helium are treated. The phenomena of contact angle hysteresis and disjoining pressure are discussed. The particular emphasis is put on recently discovered effects of superhydrophobicity and superoleophobicity.

Acknowledgements

The author is indebted to Dr. Whyman for his longstanding fruitful cooperation in the study of wetting phenomena. His critique and numerous remarks definitely improved the text. I am thankful to Professor R. Pogreb for his contribution in understanding of diversity of wetting phenomena. I want to thank my numerous MSc and PhD students for their research activity and allegiance to a spirit of scientific research. I am grateful to Mrs. Al. Musin for her kind help in editing the review. I am especially indebted to my wife Yelena Bormashenko for her inestimable help in preparing this review. I am greatly thankful to Mrs. Hanna Weiss for her valuable help in English editing of this review.

1. Plinius, *Historia Naturalis*, Lib. II, Cap. 103, John Bostock, M.D., F.R.S., H.T. Riley, Esq., B.A., Ed.
2. B. Franklin, W. Brownrigg, and R. Farish, *Philos. Trans*. **64**, 445 (1774).
3. W. Thomson (Lord Kelvin), *Philos. Mag*. **42**, 368 (1871).
4. Lord Rayleigh (J.W. Strutt), *Proc. R. Soc. London* **29**, 71 (1879).
5. A. Einstein, *Annalen der Physik* **309**, 513 (1901).
6. A. Einstein, *Naturwissenshaften* **4**, 509 (1916).
7. N. *Bohr, Philos. Trans. R. Soc. London A* **209**, 281 (1909).
8. E. Shrödinger, *Annalen der Physik* **351**, 413 (1915).
9. W. Barthlott and C. Neinhuis, *Planta* **202**, 1 (1997).
10. P.G. de Gennes, F. Brochard-Wyart, and D. Quéré, *Capillarity and Wetting Phenomena,* Springer, Berlin (2003).
11. I.M. Gelfand and S.V. Fomin, *Calculus of Variations*, Dover (2000).
12. E. Bormashenko, *Wetting of Real Surfaces, de Gruyter*, Berlin (2013).
13. Th. Young, *Philos. Trans. Royal Society of London* **95**, 65 (1805).
14. A. Marmur, *A Guide to the Equilibrium Contact Angles Maze*, in: *Contact Angle Wettability and Adhesion*, K.L. Mittal (ed.), VSP, Leiden (2009), vol. 6, p.3.
15. J. Bico, U. Thiele, and D. Quéré, *Colloids & Surf. A* **206**, 41 (2002).
16. A. Marmur, *Colloids & Surf. A* **136**, 81 (1998).
17. A Amirfazli and A.W. Neumann, *Adv. Colloid & Interface Sci.* **110**, 121 (2004).
18. A. Checco and P. Guenoun, *Phys. Rev. Lett*. **91**, 186101 (2003).
19. T. Pompe, A. Fery and S. Herminghaus, *Measurement of Contact Line Tension by Analysis of the Three-Phase Boundary with Nanometer Resolution*, in: *Apparent and Microscopic Contact Angles*, J. Drelich, J.S. Laskowski, and K.L. Mittal (eds.), VSP, Utrecht (2000), p. 3.
20. A. Aleksandrov, B. Toshev, and A. Sheludko, *Langmuir* **7**, 321 (1991).
21. A. Marmur, *J. Colloid & Interface Sci*. **186**, 462 (1997).
22. E. Bormashenko, *Colloids & Surf. A* **345**, 163 (2009).
23. J.N. Israelachvili, *Intermolecular and Surface Forces*, Elsevier, Amsterdam (2011).
24. H.Y. Erbil, *Surface Chemistry of Solid and Liquid Interfaces*, Blackwell, Oxford (2006).
25. B.V. Derjaguin and E. Obuchov, *Acta Physicochimica U.R.S.S* **5**, 1 (1936).
26. B.V. Derjaguin and N.V. Churaev, *J. Colloid & Interface Sci*. **49**, 249 (1974).
27. V.M. Starov and M.G. Velarde, *J. Phys: Condens. Matter* **21**, 464121 (2009).
28. D. Bonn and D. Ross, *Rep. Prog. Phys*. **64**, 1085 (2001).
29. C.W. Extrand and Y. Kumagai, *J. Colloid & Interface Sci*. **191**, 378 (1997).
30. C.N.C. Lam, R. Wu, D. Li, M.L. Hair, and A. W. Neumann, *Adv. Colloid & Interface Sci*. **96**, 169 (2002).
31. V.V. Yaminsky, *Hydrophobic Transitions*, in: *Apparent and Microscopic Contact Angles*, J. Drelich, J.S. Laskowski, and K.L. Mittal (eds.), VSP, Utrecht (2000), p. 47.
32. A. Marmur, *J. Colloid & Interface Sci*. **168**, 40 (1994).
33. R.E. Johnson and R.Y. Dettre, *Adv. Chemistry Series* **43**, 136 (1964).
34. M.E.R. Shanahan and A. Carre, *Langmuir* **11**, 1396 (1995).
35. D. Long, A. Ajdari, and L. Leibler, *Langmuir* **12**, 5221 (1996).
36. R. Pericet-Camara, G.K. Auernhammer, K. Koynov, S. Lorenzoni, R. Raiteri, and E. Bonaccurso, *Soft Matter* **5**, 3611 (2009).
37. O.V. Voinov, *Fluid Dynamics* **11**, 714 (1976).
38. R.L. Hoffman, *J. Colloid & Interface Sci.* **50**, 228 (1975).
39. D. Bonn, J. Eggers, J. Indekeu, J. Meunier, and E. Rolley, *Rev. Mod. Phys*. **81**, 739 (2009).
40. R.N. Wenzel, *Ind. Eng. Chem*. **28**, 988 (1936).
41. R.J. Good, *J. Am. Chem. Soc*. **74**, 5041 (1952).
42. E. Bormashenko, *J. Phys. Chem. C* **113**, 17275 (2009).
43. A.B.D. Cassie and S. Baxter, *Trans. Faraday Soc*. **40**, 546 (1944).
44. A.B.D. Cassie, *Faraday Soc*. **3**, 11 (1948).

45. M. Miwa, A. Nakajima, A. Fujishima, K. Hashimoto, and T. Watanabe, *Langmuir* **16**, 5754 (2000).
46. A. Marmur, *Langmuir* **19**, 8343 (2003).
47. T.-S. Wong and Ch.-M. Ho, *Langmuir* **25**, 12851 (2009).
48. E. Bormashenko, *J. Colloid & Interface Sci*. **360**, 317 (2011).
49. K. Koch, Bh. Bhushan, and W. Barthlott, *Progr. Mater. Sci*. **54**, 137 (2009).
50. Y.Y. Yan, N. Gao, and W. Barthlott, *Adv. Colloid & Interface Sci.* **169**, 80 (2011).
51. M.A.K. Azad, W. Barthlott, and K. Koch, *Langmuir* **31**, 13172 (2015).
52. X.-Q. Feng, X. Gao, Z. Wu, L. Jiang, and Q.-S. Zheng, *Langmuir* **23**, 4892 (2007).
53. T. Sun, L. Feng, X. Gao, and L. Jiang, *Acc. Chem. Res*. **38**, 644 (2005).
54. Y. Zheng, X. Gao, and L. Jiang, *Soft Matter* **3**, 178 (2007).
55. Ed. Bormashenko, Ye. Bormashenko, T. Stein, G. Whyman, and E. Bormashenko, *J. Colloid & Interface Sci*. **311**, 212 (2007).
56. M. Nosonovsky and Ed. Bormashenko, *Lotus Effect*: *Superhydrophobicity and Self-Cleaning*, in: *Functional Properties of Bio-Inspired Surfaces*, E.A. Favret and N.O. Fuentes (eds.), World Scientific, Singapore (2009), p. 43.
57. P. Roach, N.J. Shirtcliffe, and M.I. Newton, *Soft Matter* **4**, 224 (2008).
58. G. Ciasca, M. Papi, L. Businaro, G. Campi, M. Ortolani, V. Palmieri, A. Cedola, A. De Ninno, A. Gerardino, and G. Maulucci, *Bioinspiration & Biomimetics* **11**, 011001 (2016).
59. M. Nosonovsky, *Langmuir* **23**, 3157 (2007).
60. M. Nosonovsky and B. Bhushan, *Nano Lett*. **7**, 2633 (2007).
61. S. Herminghaus, *Europhys. Lett*. 2000 **52**, 165 (2000).
62. A.K. Kota, Y. Li, J.M. Mabry, and A. Tuteja, *Adv. Mat*. **24**, 5838 (2012).
63. H. Bellanger, Th. Darmanin, E.T. de Givenchy, and Fr. Guittard, *Chem. Rev*. **114**, 2694 (2014).
64. E. Bormashenko, R. Grynyov, G. Chaniel, H. Taitelbaum, and Ye. Bormashenko, *Appl. Surf. Sci*. **270**, 98 (2013).
65. S. Pechook, N. Kornblum, and B. Pokroy, *Adv. Funct. Mater*. **23**, 4572 (2013).
66. M. Nosonovsky and B. Bhushan, *Microelectronic Eng*. **84**, 382 (2007).
67. N.A. Patankar, *Langmuir* **26**, 8941 (2010).
68. H.J. Butt, C. Semprebon, P. Papadopoulos, D. Vollmer, M. Brinkmann, and M. Ciccotti, *Soft Matter* **9**, 418 (2013).
69. G. Whyman and E. Bormashenko, *Langmuir* **27**, 8171 (2011).
70. G. Pashos, G. Kokkoris, A.G. Papathanasiou, and A.G. Boudouvis, *J. Chem. Phys*. **144**, 034105 (2016).
71. E. Bormashenko, *Adv. Colloid & Interface Sci.* **222**, 92 (2015).
72. L. Feng, Y. Zhang, J. Xi, Y. Zhu, N. Wang, F. Xia, and L. Jiang, *Langmuir* **24**, 4114 (2008).
73. Y.I. Frenkel, *J. Exptl. Theoret. Phys. (USSR)* **18**, 659 (1948).
74. E. Bormashenko, T. Stein, R. Pogreb, and D. Aurbach, *J. Phys. Chem. C* **113**, 5568 (2009).
75. Y.M. Park, M. Gang, Y.H. Seo, and B.H. Kim, *Thin Solid Films* **520**, 362 (2011).
76. D. Quere, *Ann. Rev. Mater. Res*. **38**, 71 (2008).
77. B. Bhushan and M. Nosonovsky, *Philos. Trans. R. Soc. A* **368**, 4713 (2010).
78. H. Zhang, Y. Yu, J. Pan, S. Zhang, X. Wu, and Y. Yang, *Colloids & Surfaces A*, *Article in press* (2016).
79. A.L. Dubov, A. Mourran, M. Möller, and O.I. Vinogradova, *Appl. Phys. Lett*. **106**, 241601 (2015).
80. O. Vinogradova and A.L. Dubov, *Mendeleev Commun*. **22**, 229 (2012).
81. A. Shahraz, A. Borhan, and K.A. Fichthor, *Langmuir* **30**, 15442 (2014).
82. E.S. Savoy and P.A. Escobedo, *Langmuir* **28**, 3412 (2012).
83. E.S. Savoy and P.A. Escobedo, *Langmuir* **28**, 16080 (2012).
84. T. Koishi, K. Yasuoka, S. Fujikawa, T. Ebisuzaki, and X.C. Zeng, *Proc. Nat. Acad. Science USA* **106**, 8435 (2009).